Fatima I. Ismail [1]
Ammar T. Zakar [1]
Thoalfiqar A. Zaker [2]

[1] Department of Physics, College of Education for Pure Sciences, University of Mosul, Mosul, IRAQ
[2] Department of Laser and Spectroscopy, Laser and Photonics Centre, University of Al-Hamdaniya, Nineveh, IRAQ

Effect of Aluminum Doping on Structural and Nonlinear Optical Properties of Tin Dioxide Films Prepared by Spray Pyrolysis

This study evaluated the impact of Al doping with ratios of 3%, 5%, and 7% on the structural and non-linear optical properties of SnO_2 thin films deposited using the spray pyrolysis method. X-ray diffraction revealed a polycrystalline and tetragonal structure of the films with no phase change of the SnO_2 films. The EDX/SEM pictures reveal spherical, semi-spherical, and agglomerated nanoparticles aggregated in varied patterns and densities with Al atoms entangled inside the crystalline lattice of SnO_2. The open aperture Z- scan measurements revealed an increase in the TPA coefficient (β_{eff}) at doping levels below 7% in comparison to higher doping concentrations. Closed aperture configuration demonstrated an enhancement in the nonlinear refractive index and in turn the susceptibility $\chi^{(3)}$. The enhancement in the structural and nonlinear optical properties of SnO_2 with the doping permits its use as an alternative to ITO in the epsilon near zero and optoelectronic applications.

***Keywords*:** Transparent conductive materials; Spray pyrolysis; Tin dioxide
Received: 23 August 2024; **Revised:** 03 November; **Accepted:** 10 November 2024

1. Introduction

Materials combining both high optical transparency and electrical conductivity are known as transparent conductive materials (TCMs) [1-3]. These distinct features make TCMs indispensable in a variety of current technologies, including optoelectronics, photovoltaics, and display technologies [4]. TCMs are essential for the functionality of devices such as touch screens, advanced smart windows [5], gas sensors [6], flat panel displays [7], light-emitting diodes (LEDs) [8], and solar cells [9,10], where transparency and conductivity are critical for optimal performance and efficiency [11]. The characteristics and performance of TCMs, including Al/SnO_2, depend much on their preparation techniques. TCM thin films are made using a variety of methods, including spraying [12,13], chemical vapor deposition (CVD) [14], sol-gel processing [15], sputtering [16], and pulsed-laser deposition (PLD) [17]. Every technique has unique benefits and drawbacks that affect the final materials' optical, electrical, and structural properties [18,19].

Indium tin oxide (ITO) has traditionally been the most extensively used TCM owing to its good electrical conductivity and great transparency in the visible spectrum [20-22]. Nevertheless, ITO possesses certain notable limitations that need the exploration of substitute options. Indium is a scarce and costly element, which results in elevated expenses and raises worries over the long-term sustainability of its supply. In addition, ITO exhibits toxicity and brittleness, which restricts its applicability in flexible electronics. Further, ITO experiences significant free carrier absorption, resulting in diminished transparency within the visible spectrum and near IR range which degrade device performance [23-28]. In contrast, aluminum-doped tin oxide has demonstrated enhanced optical transparency and conductivity providing the possibility of using it as a promising alternative to ITO. This in turn leads to an improved device performance and less environmental impact [29]. Moreover, doping SnO_2 with aluminum introduces extra free carriers triggering a change from n-type to p-type conductivity. This in turn upgrades the material's electrical characteristics without considerably diminishing its optical transparency [30,31]. Thus, doping tin oxide with aluminum provides a viable avenue for modifying its characteristics as an effective alternative to ITO for a wide range of optoelectronic applications [32].

within the framework of Epsilon-Near-Zero (ENZ) materials, innovative class of materials with significantly low permittivity and unique capacity to control electromagnetic waves, the doping modifies the permittivity and nonlinear response to obtain ENZ at the appropriate operational frequencies [33]. This modification is important because it specifies the wavelength at which the substance will display ENZ properties, which has an immediate impact on the device's functionality and efficiency [7,34-37].

The aim of this study involves evaluation the structural and nonlinear optical properties of Al-doped SnO_2 (ATO) as a promising alternative of ITO in various application sectors. The investigation as well as optimization of doping methods and manufacturing procedures are crucial for enhancing the performance

and use of ATO in current technologies, notably in the photonic materials and devices.

2. Experimental Part

The pure and aluminum-doped tin oxide was prepared using spray pyrolysis method. The aqueous tin chloride was prepared through dissolving 7.0422 g of tin chloride ($SnC1_4.5H_20$) in 200 mL of distilled water. The raw material is a white powder produced by Indian General Drug House Ltd. with purity of 97.5%, 350.58 g/mol and 0.1 mol, respectively. The weight of the used material was calculated according to the following equation [38]:

$$M = \frac{Wt}{Mw}.\frac{1000}{V} \quad (1)$$

The solution was then stirred using hot plate magnetic stirrer for 20 min at a temperature of 80 °C. Similarly, same procedure was used to prepare the aqueous aluminum chloride where the 2.666 g of aluminum chloride powder was dissolved in the same amount of distilled water and stirred for 10 min at a temperature of 40°C. The two solutions then mixed together according to volumetric mixing ratios shown in table (1) and stirred for one hour at a temperature of 80°C. The mixture then sprayed on the cleaned glass substrates for 10 s with time intervals of 2 min and a temperature of 400°C.

Table (1) The volumetric mixing ratios used in the deposition process

Sample	Mixing ratio		Al doping ratio	Thin film
	Al	SnO_2		
S1	0	50	0	Pure SnO_2
S2	1.5	50	3%	Al/SnO_2
S3	2.5	50	5%	Al/SnO_2
S4	3.5	50	7%	Al/SnO_2

The nonlinearity of the sample including nonlinear refractive index and two photon absorption were obtained based on well-known z-scan technique. The samples were positioned on a computer-controlled moving rail, enabling their movement along the laser path and the focal point of the collimated beam. The laser diode beam, with wavelength of 632 nm, was collimated using 5cm-focal lens placed before the moving stage. To switch the system between open and closed configurations, the aperture with variable diameter was employed. For the closed aperture case, the diameter of the aperture was fixed around 0.5 mm. The power of the laser beam at the focal point was measured using power meter and fixed at 53 mW corresponding to intensity $I_0 = \frac{2P}{\pi w_o^2} = 156$ MW/cm^2 which shown to be enough to induce nonlinear behavior as confirmed by the results . The high power also provides the possibility of removing the contribution of the linear absorption. The transmitted signal was measured using a DET10A photodetector connected to lock-in amplifier to remove any possible noise. The spot size of the laser beam was determined according to the knife edge technique and found to be 216 µm.

3. Results and Discussion

The structural characteristics of pure and Al doped SnO_2 were analyzed based on x-ray diffraction patterns. The results showed that the pure and doped SnO_2 films were polycrystalline with a tetragonal system as shown in Fig. (1). This figure also revealed a diffraction peaks corresponding to the planes (110), (101), and (211) at diffraction angles 2θ of 51.921°, 33.560°, and 26.226°, respectively. In the prevailing direction (110), the results showed a match with the ICDD card 01-077-0448 [39]. The results indicated that the doping with aluminum did not affect the phase transformation of the SnO_2 films. The reason for the lack of effect can be attributed to the ionic radii. The chart illustrates that the peak intensities for all films diminish as doping rates increase. This phenomenon can be ascribed to the formation of atomic levels of the dopant (aluminum, in this instance) within the crystalline lattice of the host material, resulting in out-of-phase scattering of the incident x-rays at the atomic scale. Thus, the scattering of the incident x-ray for both doped and the matrix yields partially destructive interference. A small change was also noticed in the peaks locations towards small angles as the doping affects the size of the crystal and the distance between the crystal levels. The shifts in the positions of the peaks could be also attributed to the stresses resulting from the entry and spread of doping atoms in the matrix material and their possession of interstitial sites in its crystal lattice. The crystallite size (C.S.) at the full width half maximum peak (FWHM) was calculated using the Debye-Scherrer equation. The broadening of the FWHM of the peak indicates that the crystallite size decreases with increasing doping ratio as listed in table (2). The particle size within SnO_2 films is strongly influenced by the atomic radius of Al atoms, mainly due to mechanisms of atomic interactions and film formation processes. The incorporation of Al in the SnO_2 matrix may result in a decrease or an increase in the particle size depending on different parameters. The decrease in size is due to the increased rates of nucleation and the modified growth dynamics that occur during the deposition of the film. These factors promote the creation of smaller and more evenly sized particles [40]. It has been shown that the incorporation of Al alters the structural and electronic characteristics of SnO_2 through generation of extra sites inside the matrix resulting in smaller particle size [41]. Nevertheless, an excessive amount of aluminum content might result in agglomeration, which can negate the advantages of reducing the size [42].

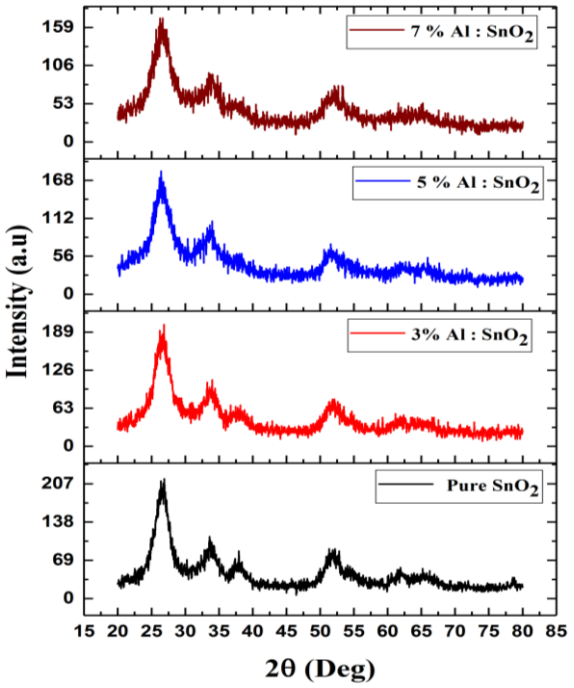

Fig. (1) XRD patterns of pure and Al-doped SnO_2 films at different doping concentrations

Figure (2) shows the SEM image of pure SnO_2 films prepared using spray pyrolysis method at 400°C. It can be seen from the figure that the average particle size is about 50-70 nm for undoped samples. The figure also indicates that the nanoparticles are mostly spherical, semi-spherical, and agglomerated, and they aggregate in different patterns and densities and the boundaries of the nanoparticles can be distinguished from the duller and darker color confirming the polycrystalline nature of the films.

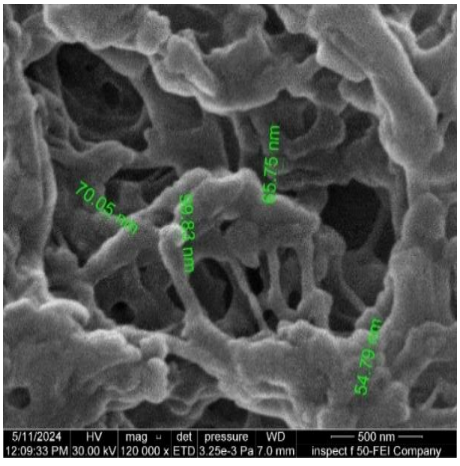

Fig. (2) The SEM image of pure SnO_2 films prepared using spray pyrolysis method at 400°C

Figure (3) shows the SEM image of 3% Al-doped SnO_2. It can be seen from the figure that the size of nanoparticles is relatively smaller than that shown in the pure counterpart. The structure of the particles is also quite similar to that of the pure sample. The structure improvement can be attributed to the lattice distortions due to the relative size difference between the Sn and Al ions, resulting in reduced particle sizes.

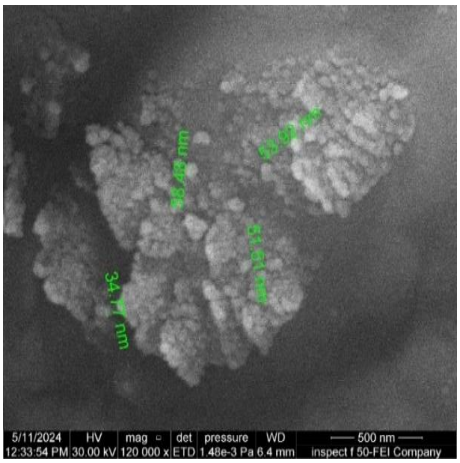

Fig. (3) The SEM image of 3% Al-doped SnO_2 deposited by spray pyrolysis method

Figure (4) shows the 5% Al-doped SnO_2 film prepared at the same deposition conditions. This figure shows an improvement in the crystallite size as the doping level is increased. The structure of the film involves spherical, semi-spherical, and agglomerated nanoparticles aggregated in different patterns and densities.

At high doping levels (>5%), the distribution and the homogeneity are enhanced as shown in Fig. (5). The inclusion of Al inside the SnO_2 lattice occurs via structural change, substitutional doping, and the existence of oxygen vacancies. This, in turn, generates lattice distortions because of the considerable size disparity between the Sn and Al ions, resulting in reduced particle sizes.

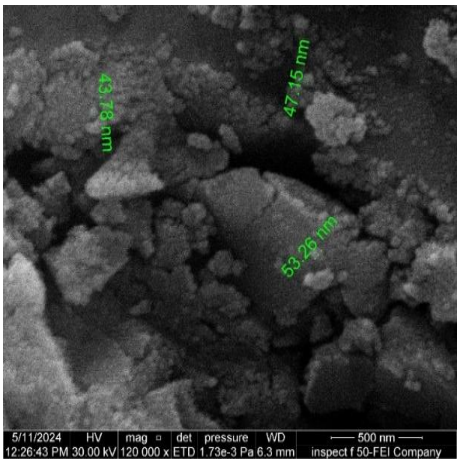

Fig. (4) The SEM image of 5% Al-doped SnO_2 deposited by spray pyrolysis method

The combination of these characteristics contributes to the improved performance of Al-doped SnO_2 films in optoelectronic applications [43]. Table (3) shows the elemental ratios for 7% Al-doped SnO_2 extracted from EDX measurements.

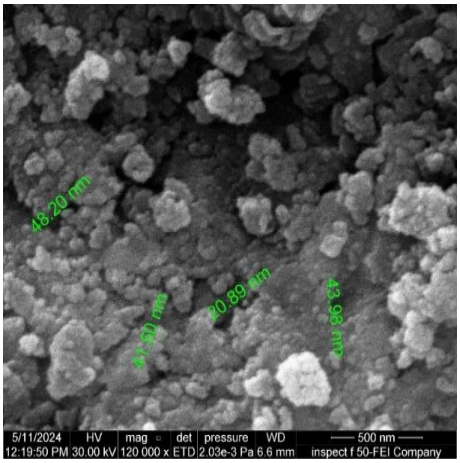

Fig. (5) The SEM image of 7% Al-doped SnO_2 deposited by spray pyrolysis method

Table (3) Elemental analysis for 7% Al-doped SnO_2 thin film sample

Element	Atomic (%)	Atomic Error (%)	Weight (%)	Weight Error (%)
O	71.1	3.1	26.9	1.2
Al	3.7	0.3	2.4	0.2
Sn	25.2	0.4	70.7	1.1

Figure (6) demonstrates EDX analysis of 7% Al-doped SnO_2 thin film. This spectrum shows different peaks which refer to the existence of the Sn and O as well as the Al inclusions with ratios 25.2%, 71.1% and 3.7% of Al, respectively, which confirms the elemental composition of Al-doped SnO_2.

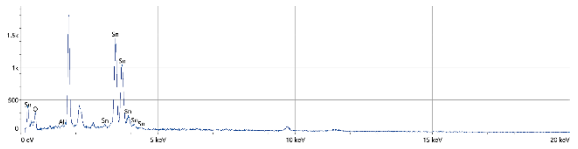

Fig. (6) EDX spectrum of 7% Al-doped SnO_2 thin film

The nonlinear optical properties of the pure and Al-doped SnO_2 were measured based on z-scan approach. This approach operates on the basis of spatial beam distortion. Depending on the type of the nonlinear process, two types of distinct peaks can be observed corresponding to close and open aperture configuration. In case of open aperture configuration, the normalized transmittance change is measured as function of the sample position with respect to the lens focus for pure SnO_2. As shown in Fig. (7), the transmittance intensity decreases as the sample approaches the focal point showing valley like trace corresponding to reverse saturation absorption (RSA). The value of the absorption coefficient (β_{eff}) is found to be 0.344 cm/W as illustrated in the table (4).

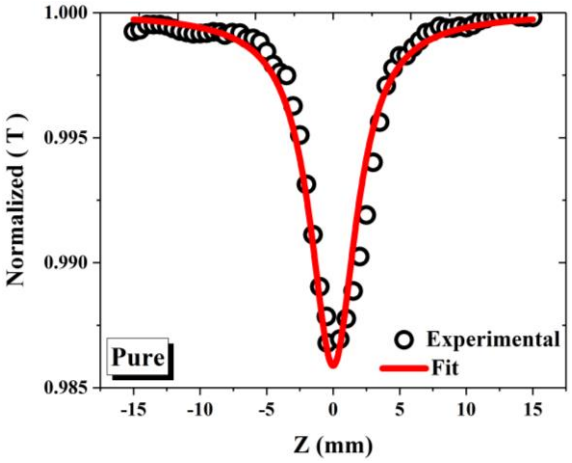

Fig. (7) The normalized transmittance of pure SnO_2 measured based on open aperture configuration

Different nonlinear processes could be responsible for such kind of absorption such as two-photon absorption (TPA), nonlinear scattering, free-carrier absorption (FCA) and the combination between all the processes. In case of semiconductors, for the TPA to occur, the photon energy should satisfy the following condition ($nhv>E_g>(n-1)hv$). Here, (hv) refers to the incident photon energy and (n) represents number of absorbed photons [44]. In this study, the excitation photon energy along the intensity axis is less than the energy gap which confirms the existence of the TPA together with other electronic effects [45,46]. In addition, if TPA is the sole mechanism that causes nonlinear absorption, the absorption coefficient βeff remains constant regardless the intensity of the excitation source along the laser beam axis.

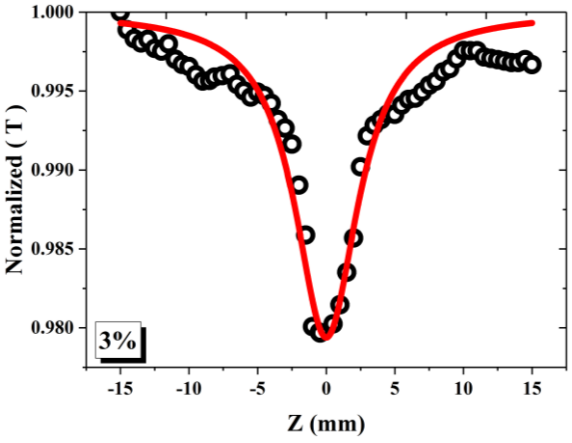

Fig. (8) The normalized transmittance of 3% Al-doped SnO_2 measured based on open aperture configuration

For low doping concentrations (<7%), shown in figures (8) and (9), the absorption coefficient (β_{eff})

enhances with increasing the doping concentration. Thus, the nonlinearity could be due to the combination of the TPA, FCA and morphology induced nonlinear scattering at these doping levels and the corresponding βeff values are shown in table (4). Figure (10) shows the normalized transmittance of 7% Al-doped SnO_2 measured based on open aperture z-scan. This figure shows a slight decrease in the absorption coefficient (β_{eff}) at 7% doping level compared to the lower doping levels which could be attributed to the Al incorporation resulting in wider energy gap which in turn reducing the possibility of TPA.

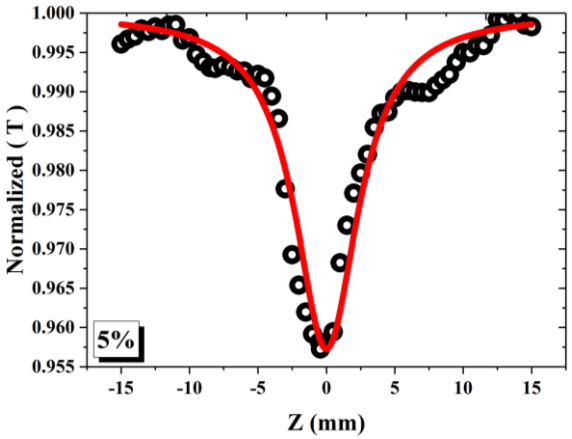

Fig. (9) The normalized transmittance of 5% Al-doped SnO_2 measured based on open aperture configuration

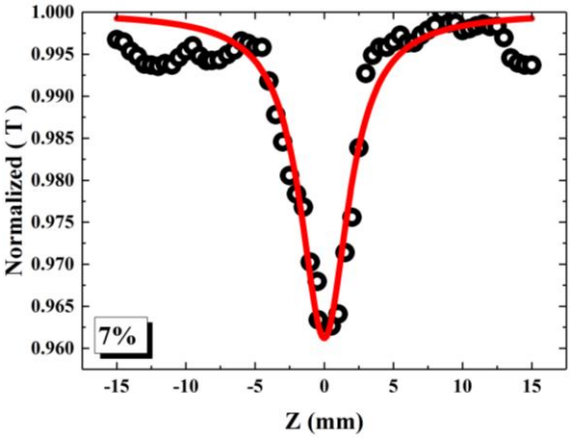

Fig. (10) The normalized transmittance of 7% Al-doped SnO_2 measured based on open aperture configuration

The drop could also be due to the deeper penetration of Al atoms in SnO_2 lattice which provides the possibility of reduced nonlinear scattering due to the crystallinity improvement of the deposited thin film as indicated earlier. The TPA coefficient values can be extracted by fitting the open aperture measurements using following equation [47]:

$$T(Z) = 1 - \left[\frac{\beta_{eff} I_o L_{eff}}{2\sqrt{2}\left(1+\frac{Z^2}{Z_o^2}\right)}\right] \qquad (2)$$

Here, Z refers to the distance between the sample and focus, I_0 (=2P/$\pi\omega_0^2$) is the laser intensity at the focal point, L_{eff}=(1-$e^{-\alpha L}$)/α is the effective length and Z_0 (=$\pi\omega_0^2/\lambda$) represents Rayleigh range. The embedded parameters α, P, ω_0 refers to absorption coefficient calculated using spectrometer at 632 nm wavelength, laser power and the waist length, respectively. The extracted values of TPA coefficient (β_{eff}) are shown in table (4).

In the case of closed aperture, the nonlinear refractive index was calculated based on the change between intensity of the peak and valley as indicated in the following equation [47]:

$$n_2 = \frac{1}{0.405(1-S)^{0.25} K I_o L_{eff}} \Delta T_{P-V} \qquad (3)$$

where $S = \left(1 - e^{-\frac{2r^2}{\omega^2}}\right)$ can be calculated based on aperture and beam diameters while K represents the wavenumber

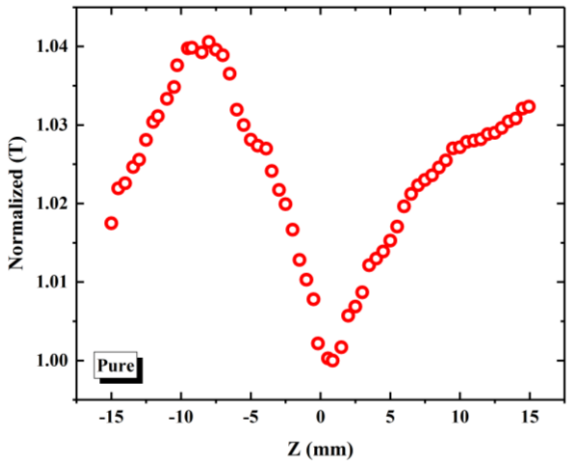

Fig. (11) The normalized transmittance of pure SnO_2 film measured based on closed aperture configuration

Figure (11) shows the normalized transmittance of pure tin dioxide measured based on closed aperture configuration from which the nonlinear refractive index was calculated and listed in table (3). This figure also indicates that the peak is trailed by the valley. This in turn reveals a negative phase shift (self-defocusing) behavior of the pure film. The peak to valley separation is larger the Rayleigh range Z_0 indicating the thermal induced nonlinearity of the refractive index as well as the third order process.

The absolute value together with the real and the imaginary parts of the nonlinear susceptibility can be calculated by substituting n_2 and β_{eff} in the following expressions [47]:

$$Re\chi^{(3)}(esu) = 10^{-4} \times \frac{\varepsilon_o c^2 n_o^2 n_2}{\pi}\left(\frac{cm^2}{W}\right) \qquad (4)$$

$$Im\chi^{(3)}(esu) = 10^{-2} \times \frac{\varepsilon_o c^2 n_o^2 \lambda \beta_{eff}}{4\pi^2}\left(\frac{cm}{W}\right) \qquad (5)$$

$$|\chi^3| = \sqrt{(Re\chi^{(3)})^2 + (Im\chi^{(3)})^2} \quad (esu) \qquad (6)$$

For doping levels less than 7% as shown in figures (12) and (13), the normalized transmittance measured

based on closed aperture configuration revealed a similar peak to valley trend indicating the self-defocusing of both films. These figures demonstrated an enhancement in the nonlinear refractive index (n_2) as well as the nonlinear susceptibility. This could be due to Al doping that acts as p-type dopant providing the possibility of further generation of ions that takes part in nonlinear processes.

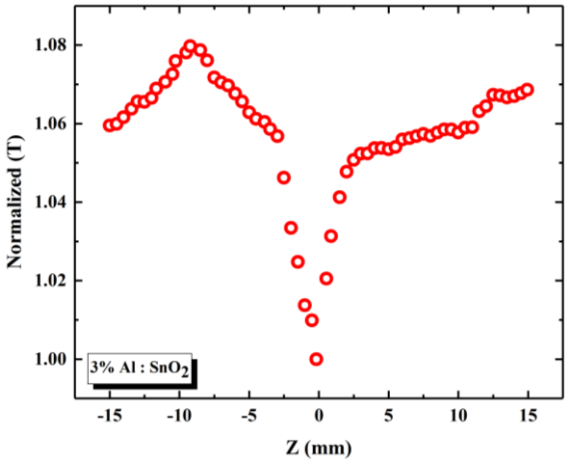

Fig. (12) The normalized transmittance of 3% Al-doped SnO_2 film measured based on closed aperture configuration

It also shown that the higher crystallite size yields weaker quantum confinement, such that, as the temperature rises and the crystallite size improves the interaction between the photon energy and nanocrystallites increases yielding an enhancement in the nonlinear susceptibility [48].

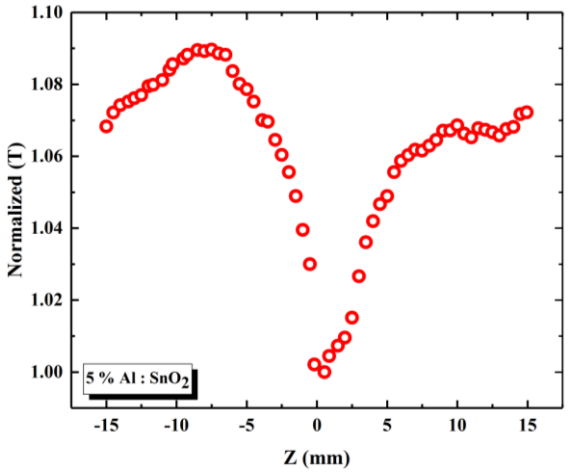

Fig. (13) The normalized transmittance of 5% Al-doped SnO_2 film measured based on closed aperture configuration

At doping levels greater than 5% shown in Fig. (14), the normalized transmittance also follows peak to valley trend with rather enhancement in the nonlinear refractive index as well as the nonlinear susceptibility as shown in Fig. (4). This could attributed to doping induced ions that takes part in nonlinear processes. This could be due to crystallite size improvement which increases the interaction between the photon energy and nanocrystallites yielding a nonlinear susceptibility enhancement.

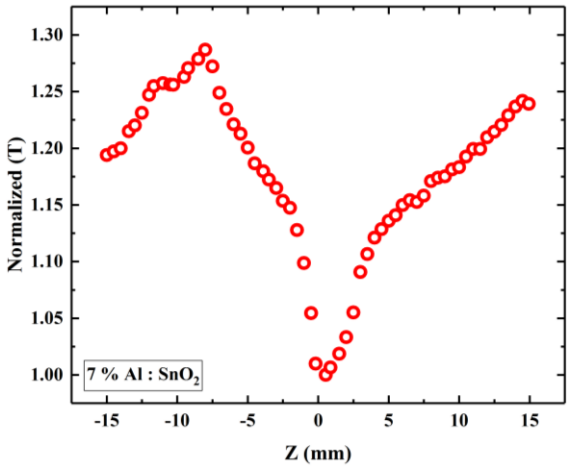

Fig. (13) The normalized transmittance of 7% Al-doped SnO_2 film measured based on closed aperture configuration.

4. Conclusion

Pure and Al-doped tin oxide thin films at 3%, 5%, and 7% doping concentrations were deposited by spray pyrolysis method. The polycrystalline and tetragonal structure of the doped and undoped films were confirmed. Spherical, semi-spherical, and agglomerated nanoparticles with Al atoms interwoven in the SnO_2 crystalline lattice were revealed. The open aperture z-scan measurements showed an enhancement in the TPA coefficient β_{eff} within the range of 0.344-0.947 cm/W with increasing doping levels. Closed aperture configuration revealed that the nonlinear refractive index is also increases from $0.969x10^{-8}$ to $5.25x10^{-8}$ cm^2/W with increasing doping concentration. The findings showed an increase in the absolute value and real and imaginary parts of nonlinear susceptibility $\chi^{(3)}$. The structural and nonlinear enhancement nominate Al-doped SnO_2 as a promising alternative of ITO in the field of photonic materials and devices.

References

[1] A.M. Ganose and D.O. Scanlon, "Band gap and work function tailoring of SnO_2 for improved transparent conducting ability in photovoltaics", *J. Mater. Chem. C*, 4(7) (2016) 1467-1475.

[2] R. Ramarajan et al., "Enhanced optical transparency and electrical conductivity of Ba and Sb co-doped SnO_2 thin films", *J. Alloys Comp.*, 823 (2020) 153709.

[3] Y. Mouchaal and A.J. Khelil, "Optimization of SnO_2/Ag nanowire transparent hybrid electrodes for optoelectronic applications", *Euro. Phys. J. Appl. Phys.*, 87(3) (2019) 31302.

[4] A. Abdel-Galil, N. Moussa and I.J. Yahia, "Synthesis and optical characterization of

nanocrystalline fluorine-doped tin oxide films: conductive window layer for optoelectronic applications", *Appl. Phys. A*, 127(6) (2021) 474.
[5] T.D. Nguyen et al., "Efficient near infrared modulation with high visible transparency using SnO_2–WO_3 nanostructure for advanced smart windows", *Adv. Opt. Mater.*, 7(8) (2019) 1801389.
[6] H.K. Saglam et al., "Growth of Transparent Conductive Oxide SnO_2 Thin Film as H_2 Sensor", *Int. J. Innov. Res. Rev.*, 5(2) (2021) 69-73.
[7] N. Kinsey et al., "Epsilon-near-zero Al-doped ZnO for ultrafast switching at telecom wavelengths", *Optica*, 2(7) (2015) 616-622.
[8] Y. Jo, C. Hong and J.J. Kwak, "Improved electrical and optical properties of ITO thin films by using electron beam irradiation and their application to UV-LED as highly transparent p-type electrodes", *Curr. Appl. Phys.*, 11(4) (2011) S143-S146.
[9] L. Xiong et al., "Review on the application of SnO2 in perovskite solar cells", *Adv. Func. Mater.*, 28(35) (2018) 1802757.
[10] S.H. Lee et al., "Transparent, homogeneous tin oxide (SnO_2) thin films containing SnO_2-coated gold nanoparticles", *Chem. Mater.*, 25(23) (2013) 4697-4702.
[11] R. Majumder et al., "Self-doped SnO_2: F synthesis by aerosol-spray deposition technique and their application in relative humidity sensor devices", *Appl. Nanosci.*, 9 (2019) 1553-1563.
[12] L. Wang et al., "Effect of F and Nb co-doping on structural, electrical and optical properties of spray deposited tin oxide thin films", *Thin Solid Films*, 649 (2018) 147-153.
[13] G. Turgut and E.J. Sönmez, "Synthesis and characterization of Mo doped SnO_2 thin films with spray pyrolysis", *Superlatt. Microstruct.*, 69 (2014) 175-186.
[14] S. Yu et al., "Transparent conducting Sb-doped SnO_2 thin films grown by pulsed laser deposition", *J. Non-cryst. Solids*, 358(23) (2012) 3137-3140.
[15] K. Selma et al., "Investigation of UV photosensor properties of Al-doped SnO_2 thin films deposited by sol-gel dip-coating method", *J. Semicond.*, 44(3) (2023) 032801.
[16] H.S. So et al., "Optical properties of amorphous and crystalline Sb-doped SnO_2 thin films studied with spectroscopic ellipsometry: optical gap energy and effective mass", *J. Appl. Phys.*, 118(8) (2015) 085303.
[17] X. Xiao et al., "Optical and electrical properties of SnO_2:Sb thin films deposited by oblique angle deposition", *Appl. Surf. Sci.*, 256(6) (2010) 1636-1640.
[18] J. Montero et al., "Preparation of reactively sputtered Sb-doped SnO_2 thin films: Structural, electrical and optical properties", *Solar Ener. Mater. Solar Cells*, 94(3) (2010) 612-616.
[19] E. Elangovan, K. Ramesh and K.J. Ramamurthi, "Studies on the structural and electrical properties of spray deposited SnO_2:Sb thin films as a function of substrate temperature", *Solid State Commun.*, 130(8) (2004) 523-527.
[20] A. Wang et al., "Effects of doping and annealing on properties of ZnO films grown by atomic layer deposition", *Nanoscale Res. Lett.*, 10 (2015) 1-10.
[21] H.J. Cho et al., "The effect of annealing on Al-doped ZnO films deposited by RF magnetron sputtering method for transparent electrodes", *Thin Solid Films*, 518(11) (2010) 2941-2944.
[22] G. Mei-Zhen et al., "Effect of annealing conditions on properties of sol-gel derived Al-doped ZnO thin films", *Chinese Phys. Lett.*, 26(8) (2009) 088105.
[23] M. Kambe et al., "Improvement of a-Si solar cell properties by using SnO_2:F TCO films coated with an ultra-thin TiO_2 layer prepared by APCVD", *Solar Ener. Mater. Solar Cells*, 90(18-19) (2006) 3014-3020.
[24] Y. Yang et al., "Highly transparent and conductive double-layer oxide thin films as anodes for organic light-emitting diodes", *Appl. Phys. Lett.*, 89(5) (2006) 051116.
[25] A.N. Tiwari et al., "CdTe solar cell in a novel configuration", *Prog. Photovolt. Res. Appl.*, 12(1) (2004) 33-38.
[26] I. Hamberg and C.G. Granqvist, "Evaporated Sn-doped In_2O_3 films: Basic optical properties and applications to energy-efficient windows", *J. Appl. Phys.*, 60(11) (1986) R123-R160.
[27] A. Porch et al., "Electromagnetic absorption in transparent conducting films", *J. Appl. Phys.*, 95(9) (2004) 4734-4737.
[28] P. Sivakumar et al., "Effect of Ti doping on structural, optical and electrical properties of SnO_2 transparent conducting thin films deposited by sol-gel spin coating", *Opt. Mater.*, 113 (2021) 110845.
[29] R. Bel Hadj Tahar et al., "Tin doped indium oxide thin films: Electrical properties", *J. Appl. Phys.*, 83(5) (1998) 2631-2645.
[30] P.-M. Lee et al., "Experimental observation and computer simulation of Al/Sn substitution in p-type aluminum nitride-doped tin oxide thin film", *J. Phys. Chem. C*, 120(8) (2016) 4211-4218.
[31] S. Soumya, R. Vinodkumar and N.J. Unnikrishnan, "Conductivity type inversion and optical properties of aluminium doped SnO_2 thin films prepared by sol-gel spin coating technique", *J. Sol-Gel Sci. Technol.*, 99(3) (2021) 636-649.
[32] G.K. Dalapati et al., "Tin oxide for optoelectronic, photovoltaic and energy storage devices: a review", *J. Mater. Chem. A*, 9(31) (2021) 16621-16684.

[33] J. Bohn et al., "All-optical switching of an epsilon-near-zero plasmon resonance in indium tin oxide", *Nature Commun.*, 12(1) (2021) 1017.
[34] M. Silveirinha and N.J. Engheta, "Tunneling of Electromagnetic Energy through Subwavelength Channels and Bends using ε-Near-Zero Materials", *Phys. Rev. Lett.*, 97(15) (2006) 157403.
[35] S. Molesky, C.J. Dewalt and Z.J. Jacob, "High temperature epsilon-near-zero and epsilon-near-pole metamaterial emitters for thermophotovoltaics", *Opt. Exp.*, 21(101) (2013) A96-A110.
[36] X. Niu et al., "Epsilon-near-zero photonics: a new platform for integrated devices", *Opt. Mater.*, 6(10) (2018) 1701292.
[37] O. Reshef et al., "Nonlinear optical effects in epsilon-near-zero media", *Nature Rev. Mater.*, 4(8) (2019) 535-551.
[38] J.N. Jensen, **"A problem-solving approach to aquatic chemistry"**, John Wiley & Sons (2023).
[39] S. Gates-Rector and T.J.P.D. Blanton, "The powder diffraction file: a quality materials characterization database", *Powder Diffract.*, 34(4) (2019) 352-360.
[40] G.K. Deyu et al., "SnO_2 films deposited by ultrasonic spray pyrolysis: influence of al incorporation on the properties", *Molecules*, 24(15) (2019) 2797.
[41] A.R. Razeghizadeh et al., "Growth and optical properties investigation of pure and Al-doped SnO_2 nanostructures by sol-gel method", *Iranian J. Chem. Chem. Eng.*, 366(5) (2015) 1-8.
[42] I. Saoula et al., "Effect of (Al, Zn, Cu, and Sr) doping on structural, optical and electrical properties of sprayed SnO_2 thin films", *Acta Metallurgica Slovaca*, 29(2) (2023) 59-62.
[43] B. Salameh et al., "Optoelectronic properties and optical transitions in low concentrated aluminum-doped tin oxide thin films", *J. Alloys Comp.*, 969 (2023) 172412.
[44] L. Kamath et al., "Preparation, characterization and study on the nonlinear optical parameters of novel biphenyl-4-carbohydrazide derivative", *Materials Today: Proc.*, 35 (2021) 478-482.
[45] Z.Y. Banyamin et al., "Electrical and optical properties of fluorine doped tin oxide thin films prepared by magnetron sputtering", *Coatings*, 4(4) (2014) 732-746.
[46] S. Chacko, M.J. Bushiri and V.J. Vaidyan, "Photoluminescence studies of spray pyrolytically grown nanostructured tin oxide semiconductor thin films on glass substrates", *J. Phys. D: Appl. Phys.*, 39(21) (2006) 4540.
[47] R.W. Boyd, A.L. Gaeta and E. Giese, **"Nonlinear Optics"**, Springer Handbook of Atomic, Molecular, and Optical Physics, Springer (2008), pp. 1097-1110.
[48] L. Irimpan et al., "Size-dependent enhancement of nonlinear optical properties in nanocolloids of ZnO", *J. Appl. Phys.*, 103(3) (2008) 033105.

Table (2) The crystallite size, Miller indices, the inter-planar distance, and the FWHM of the peaks and diffraction angles

Sample	2θ (deg)	FWHM (deg)	d_{hkl} Exp. (Å)	d_{hkl} Std. (Å)	(hkl)	C.S. (nm)
Pure SnO_2	26.2265	0.2361	3.2746	3.3510	110	32.6816
	33.5608	0.2180	2.4578	2.6445	101	34.5764
	51.9217	0.1587	1.6718	1.7647	211	44.3953
3% Al_2O_3	26.5141	0.3148	3.2418	3.3510	110	24.4962
	33.1528	0.3148	2.4846	2.6445	101	23.9749
	51.3594	0.2180	1.6877	1.7647	211	32.3932
5% Al_2O_3	26.2985	0.3936	3.2669	3.3510	110	19.6060
	33.1753	0.3148	2.4831	2.6445	101	24.1805
	51.3087	0.2780	1.6892	1.7647	211	25.6713
7% Al_2O_3	26.6723	0.4723	3.2237	3.3510	110	16.3727
	33.2169	0.6297	2.4803	2.6445	101	11.9867
	51.0401	0.6146	1.6998	1.7647	211	11.4960

Table (4) The nonlinear optical parameters of pure and Al-doped SnO_2 films

Sample	n_2 x10^{-8} (cm/W)	β_{eff} (cm/W)	Re[$\chi^{(3)}$] x10^{-6} (esu)	Im [$\chi^{(3)}$] x10^{-3} (esu)	$\chi^{(3)}$ x10^{-8} (esu)
Pure SnO_2	0.969	0.344	0.481	8.4	0.40
3% Al_2O_3	1.880	0.451	1.044	12.3	1.28
5% Al_2O_3	2.090	0.954	1.192	26.7	3.18
7% Al_2O_3	5.250	0.947	5.848	34.0	13.08

